Supporting Information

Tagliazucchi et al. 10.1073/pnas.1406122111

SI Text

The Bond-Order Parameters Are Good Descriptors of the Morphology of the System

To show that the bond-order parameters are good descriptors of the morphology and order of the system, we determined the bond-order parameters averaged over one period (as defined in Eq. **5** in the main text) in all of the simulations used to construct the morphology diagram in Fig. 3 *B*, *i* (linear pH–time program) of the main text. For each point in the morphology diagram (i.e., each C, ρ pair), we determined $\langle\overline{\psi}_n\rangle_\tau$ for $n = 1$, 2, 3, and 4. If all these values were smaller than 0.5, we assigned the point in the diagram to the disordered morphology; otherwise, we chose the n having the largest $\langle\overline{\psi}_n\rangle_\tau$ and assigned the structure according to it: dimers for $n = 1$, fibers for $n = 2$, honeycomb for $n = 3$, and square lattice for $n = 4$. In Fig. S2 we compare the phase diagram constructed following this method (Fig. S2*A*) to that obtained by visual inspection of the morphologies (Fig. S2*B*, also shown in Fig. 3 *B*, *i* of the main text). These morphology diagrams are in good agreement; therefore, we are confident in the use of $\overline{\psi}_n$ as a descriptor of the morphology and order of the system.

Asymptotic Behavior of the System in the Limit of Fast Oscillations

In this section, we study the asymptotic behavior of the system in the limit of fast oscillation by performing a perturbation analysis on the Fokker–Planck equation of the system. This analysis is based on the work of Reimann et al. (1) and Reimann (2) on thermal flashing ratchets. The Fokker–Planck equation of a system of particles interacting via time-oscillating potentials is

$$\frac{\partial p(\mathbf{r},t)}{\partial t} = D\nabla\left[\left(p(\mathbf{r},t)\nabla\beta U(\mathbf{r},t) + \nabla p(\mathbf{r},t)\right)\right], \qquad \text{[S1]}$$

where D is the diffusion constant of the particles (assumed to be position and time independent and the same for all particles), $\mathbf{r}$ is a $2N$ vector describing the position of the N particles in the system, $p(\mathbf{r}, t)$ is the probability density at time t (i.e., the probability of finding the system at $\mathbf{r}$ at time t), $U(\mathbf{r}, t)$ is the total potential energy of a system at $\mathbf{r}$ and time t, and $\nabla = \sum_i^{2N}(\partial/\partial r_i)$.

In an equilibrium (nonoscillating) system, both the potential energy and the probability density are independent of time; therefore,

$$D\nabla\left[\left(p(\mathbf{r})\nabla\beta U(\mathbf{r}) + \nabla p(\mathbf{r})\right)\right] = 0, \qquad \text{[S2]}$$

which—as expected—yields the Boltzmann distribution upon solving for $p(\mathbf{r})$:

$$p(\mathbf{r}) = \frac{\exp\left(-\beta U(\mathbf{r})\right)}{\int d\mathbf{r}\exp\left(-\beta U(\mathbf{r})\right)}. \qquad \text{[S3]}$$

Let us analyze now a periodic nonequilibrium steady state where the interparticle potentials oscillate with period τ. In such a system, $p(\mathbf{r}, t) = p(\mathbf{r}, t + n\tau)$ for any integer n. We define $h = t/\tau$ and the probability of finding the system at position $\mathbf{r}$ and stage h as $\rho^\tau(\mathbf{r}, h)$. Using this convention, Eq. **S1** becomes

$$\frac{\partial\rho^\tau(\mathbf{r},h)}{\partial h} = \tau D\nabla[(\rho^\tau(\mathbf{r},h)\nabla\beta U(\mathbf{r},h) + \nabla\rho^\tau(\mathbf{r},h))]. \qquad \text{[S4]}$$

Eq. **S4** has no simple analytical solution, but we can consider the asymptotic limit $\tau \to 0$. Let us decompose $\rho^\tau(\mathbf{r}, h)$ as a power series in τ,

$$\rho^\tau(\mathbf{r},h) = \sum_{n=0}^{\infty}\tau^n\rho_n(\mathbf{r},h), \qquad \text{[S5]}$$

where the functions $\rho_n(\mathbf{r}, h)$ are independent of τ. We are interested in an expression for $\rho_0(\mathbf{r}, h)$ because in the limit of $\tau \to 0$, $\rho^\tau(\mathbf{r}, h) \to \rho_0(\mathbf{r}, h)$. Note that the $\rho_n(\mathbf{r}, h)$ functions are periodic in time and thus fulfill the condition

$$\rho_n(\mathbf{r},0) = \rho_n(\mathbf{r},1). \qquad \text{[S6]}$$

We now replace Eq. **S5** into Eq. **S4**. Because the Fokker–Planck equation is valid for an arbitrary τ, terms of the same power of τ on both sides of the equation should be equal. This condition results in the following equations for the zeroth and first-order terms in τ:

$$\frac{\partial\rho_0(\mathbf{r},h)}{\partial h} = 0 \qquad \text{[S7]}$$

$$\frac{\partial\rho_1(\mathbf{r},h)}{\partial h} = D\nabla\left[\left(\rho_0(\mathbf{r},h)\nabla\beta U(\mathbf{r},h) + \nabla\rho_0(\mathbf{r},h)\right)\right]. \qquad \text{[S8]}$$

We can integrate Eq. **S8** between $h = 0$ and $h = 1$ and use the fact that ρ_0 is independent of h (condition given by Eq. **S7**) and Eq. **S6** to get

$$D\nabla\left[\left(\rho_0(\mathbf{r})\nabla\left(\int_0^1 dh\beta U(\mathbf{r},h)\right) + \nabla\rho_0(\mathbf{r})\right)\right] = 0. \qquad \text{[S9]}$$

Finally, Eq. **S9** can be solved analytically to yield

$$p_0(\mathbf{r}) = \frac{\exp\left(-\int_0^1 dh\beta U(\mathbf{r},h)\right)}{\int d\mathbf{r}\exp\left(-\int_0^1 dh\beta U(\mathbf{r},h)\right)}. \qquad \text{[S10]}$$

Comparison between Eq. **S3** (equilibrium) and Eq. **S10** (periodic steady state) shows that in the limit $\tau \to 0$ and a periodic steady-state condition, the system of particles interacting via oscillating interparticle potentials is equivalent to an equilibrium system of particles interacting via an effective average potential, given by

$$U^{\text{eff}}(\mathbf{r}) = \int_0^1 U(\mathbf{r},h)dh. \qquad \text{[S11]}$$

We finally decompose the total potential energy in Eq. **S11** into its contributions (in the present case, U is pairwise additive):

$$\sum_{i,j>i}u_{ij}^{\text{eff}}\left(|\mathbf{r}_i - \mathbf{r}_j|\right) = \sum_{i,j>i}\int_0^1 u_{ij}\left(|\mathbf{r}_i - \mathbf{r}_j|,h\right)dh. \qquad \text{[S12]}$$

For Eq. **S12** to be valid for any arbitrary set of functions $u_{ij}(|\mathbf{r}_i - \mathbf{r}_j|, h)$, the following condition must hold:

$$u_{ij}^{\text{eff}}(|\mathbf{r}_i-\mathbf{r}_j|)=\int_0^1 u_{ij}(|\mathbf{r}_i-\mathbf{r}_j|,h)dh. \quad \text{[S13]}$$

This equation is equivalent to Eq. **5** in the main text.

Comparison of Radial Distribution Functions Obtained in Simulations with Time-Oscillating Potentials and the Effective Time-Averaged Potential

We determined the pair correlation functions for *aa*, *ab*, and *bb* pairs from simulations, using oscillatory potentials as well as the effective time-averaged potential defined by Eq. **5** in the main text. In the case of the oscillatory potential, we averaged the pair correlation function over one oscillation period. See Fig. S3.

Calculation of the Characteristic Diffusional Timescale, t_d, as a Function of the Size of the Colloid

We start from the definition of the diffusion coefficient,

$$D=\frac{k_BT}{6\pi\eta(\sigma/2)}, \quad \text{[S14]}$$

and the diffusional timescale,

$$t_d=\frac{\sigma^2}{D}. \quad \text{[S15]}$$

In water at 298 K, $D\sim(0.44\ \mu m^3\cdot s^{-1})\cdot\sigma^{-1}$, and thus combining Eqs. **S14** and **S15** yields

$$t_d=\frac{\sigma^3}{0.44\ \mu m^3}s. \quad \text{[S16]}$$

We used Eq. **S16** to determine the values of t_d as a function of σ shown in Table S1.

Determination of the Energy Dissipation Rate from the Brownian Dynamics Simulations

The instantaneous change in the total energy of the system is the sum of the energy dissipated by the system into the environment and the work performed on the system by changing the interparticle potentials. In a periodic nonequilibrium steady state, the change in total energy during one oscillation cycle is zero and, therefore, the statistically averaged energy dissipated per period (ε_d) is equal to the negative of the statistically averaged energy performed on the system per period (ε_w), which is given by (3)

$$\varepsilon_d=-\varepsilon_w=-\lim_{M\to\infty}\frac{1}{M}\sum_{m=1}^{M}\int_0^\tau\left.\frac{\partial U(\mathbf{r},t+m\tau)}{\partial t}\right|_{\mathbf{r}}dt. \quad \text{[S17]}$$

In Eq. **S17**, $U(\mathbf{r}, t)$ is the total potential energy of the system at time t and particle positions $\mathbf{r}$. In our Brownian dynamics (BD) implementation we calculate the time derivative of U by dividing each BD time step into two processes: First we update the interactions between particles and then we move them. The time derivative of U at constant $\mathbf{r}$ is the difference between the potential energy at the beginning of the time step (before updating interactions) and that after updating the interactions (but before moving the particles).

Analysis of Energy Dissipation in the Limit of Very Fast Oscillations

We start our analysis with Eq. **S17**. The interactions between particles are pairwise additive; therefore, we can write

$$U(\mathbf{r},t)=\sum_{i,j>i}u_{ij}(|\mathbf{r}_i-\mathbf{r}_j|,t). \quad \text{[S18]}$$

We then split the summation in Eq. **S18** into three sums corresponding to *aa*, *ab*, and *bb* interactions:

$$U(\mathbf{r},t)=\sum_{i,j>i}^{i,j\in a}u_{aa}(|\mathbf{r}_i-\mathbf{r}_j|,t)+\sum_{i,j}^{i\in a,j\in b}u_{ab}(|\mathbf{r}_i-\mathbf{r}_j|,t)+\sum_{i,j>i}^{i,j\in b}u_{bb}(|\mathbf{r}_i-\mathbf{r}_j|,t). \quad \text{[S19]}$$

Replacing Eq. **S19** into Eq. **S17**, we get

$$\begin{aligned}\varepsilon_d=&-\lim_{M\to\infty}\frac{1}{M}\sum_{m=1}^{M}\sum_{i,j>i}^{i,j\in a}\int_0^\tau\left.\frac{\partial u_{aa}(|\mathbf{r}_i-\mathbf{r}_j|,t+m\tau)}{\partial t}\right|_{\mathbf{r}}dt\\&-\lim_{M\to\infty}\frac{1}{M}\sum_{m=1}^{M}\sum_{i,j}^{i\in a,j\in b}\int_0^\tau\left.\frac{\partial u_{ab}(|\mathbf{r}_i-\mathbf{r}_j|,t+m\tau)}{\partial t}\right|_{\mathbf{r}}dt\\&-\lim_{M\to\infty}\frac{1}{M}\sum_{m=1}^{M}\sum_{i,j>i}^{i,j\in b}\int_0^\tau\left.\frac{\partial u_{bb}(|\mathbf{r}_i-\mathbf{r}_j|,t+m\tau)}{\partial t}\right|_{\mathbf{r}}dt.\end{aligned} \quad \text{[S20]}$$

Let us consider only the first term of Eq. **S20**, which we denote ε_d^{aa}. In the periodic nonequilibrium steady state, the average properties of the system depend only on the stage within the period (h, *Asymptotic Behavior of the System in the Limit of Fast Oscillations* section) but do not change with the number of the period (m). For the observable $A(h)$, we define the average value $\langle A(h)\rangle$ (with $0<h<1$) as

$$\langle A(h)\rangle=-\lim_{M\to\infty}\frac{1}{M}\sum_{m=1}^{M}A(h\tau+m\tau). \quad \text{[S21]}$$

Using the definition in Eq. **S21** and the change of variables $t=h\tau$, we can write

$$\varepsilon_d^{aa}=-\sum_{i,j>i}^{i,j\in a}\int_0^1\left\langle\left.\frac{\partial u_{aa}(|\mathbf{r}_i-\mathbf{r}_j|,h)}{\partial h}\right|_{\mathbf{r}}\right\rangle dh. \quad \text{[S22]}$$

For a given value of h, the term $\langle\partial u_{aa}(|\mathbf{r}_i-\mathbf{r}_j|,h)/\partial h|_{\mathbf{r}}\rangle$ is the same for any i, j pair of a particles. We can, therefore, rewrite the summation in Eq. **S22** to obtain

$$\varepsilon_d^{aa}=-\frac{N_a^2}{2}\int_0^1\left\langle\left.\frac{\partial u_{aa}(|\mathbf{r}_1-\mathbf{r}_2|,h)}{\partial h}\right|_{\mathbf{r}}\right\rangle dh. \quad \text{[S23]}$$

Eq. **S23** can be rewritten as

$$\varepsilon_d^{aa}=-\frac{N_a^2}{2}\int d\mathbf{r}_1\int d\mathbf{r}_2\int_0^1 dh\frac{\partial u_{aa}(|\mathbf{r}_1-\mathbf{r}_2|,h)}{\partial h}\rho_{aa}^{ss}(\mathbf{r}_1,\mathbf{r}_2,h), \quad \text{[S24]}$$

where N_a is the number of particles of type a and $\rho_{aa}^{ss}(\mathbf{r}_1, \mathbf{r}_2, h)$ $d\mathbf{r}_1d\mathbf{r}_2$ is the probability of finding particle 1 between $\mathbf{r}_1$ and $\mathbf{r}_1+d\mathbf{r}_1$ and particle 2 between $\mathbf{r}_2$ and $\mathbf{r}_2+d\mathbf{r}_2$ when the period is at stage h (the superindex ss denotes the periodic steady-state

condition). Because our system is isotropic, we define $r = |\mathbf{r}_1 - \mathbf{r}_2|$. We also define $g^{ss}_{aa}(r, h)dr$ as the average number of particles of type a located at a distance between r and $r + dr$ from a particle of type a at stage h. Applying these definitions to Eq. **S24**, we obtain

$$\varepsilon_d^{aa} = -\frac{N_a}{2}\int dr \int_0^1 dh \frac{\partial u_{aa}(r,h)}{\partial h} g^{ss}_{aa}(r,h). \qquad \textbf{[S25]}$$

In the limit $\tau \to 0$, the structure of the system is described by an effective potential (*Asymptotic Behavior of the System in the Limit of Fast Oscillations* section) and, therefore, $g^{ss}_{aa}(r, h)$ is equal to the pair correlation function between a particles of the effective potential, $g^{eff}_{aa}(r)$ (pair correlation functions in Fig. S3). Replacing $g^{ss}_{aa}(r, h)$ by $g^{eff}_{aa}(r)$ in Eq. **S25** yields

$$\varepsilon_d^{aa} = -\frac{N_a}{2}\int dr\ g^{\text{eff}}_{aa}(r) \int_0^1 dh \frac{\partial u_{aa}(r,h)}{\partial h}. \qquad \textbf{[S26]}$$

Evaluating the inner integral over h yields

$$\varepsilon_d^{aa} = -\frac{N_a}{2}\int dr\ g^{\text{eff}}_{aa}(r)\left[u_{aa}(r,1) - u_{aa}(r,0)\right], \qquad \textbf{[S27]}$$

which vanishes because $u_{aa}(r,1) = u_{aa}(r,0)$. The same argument can be applied to the second and third terms in Eq. **S20**, which finally proves that $\varepsilon_d \to 0$ for $\tau \to 0$.

It is important to note that whereas the energy dissipation per oscillation period, ε_d, vanishes for $\tau \to 0$, our argument provides no information on the behavior of the energy dissipation per unit time, ε_d/τ.

Analysis of Energy Dissipation in the Limit of Very Slow Oscillations

In the limit of very slow oscillations, the system can relax completely at every stage of the cycle; therefore $g^{ss}_{aa}(r, h)$ in Eq. **S25** is equal to the pair correlation function between a particles for an equilibrium system at h [i.e., a system with pH = pH(h)], $g^{eq}_{aa}(r, h)$. Therefore, Eq. **S25** becomes

$$\varepsilon_d^{aa} = -\frac{N_a}{2}\int dr \int_0^1 dh \frac{\partial u_{aa}(r,h)}{\partial h} g^{\text{eq}}_{aa}(r,h). \qquad \textbf{[S28]}$$

Oscillating potentials that are h reversible, such as those used in this work and shown in Fig. 3 in the main text, fulfill the condition

$$u_{ij}(r,h) = u_{ij}(r,1-h). \qquad \textbf{[S29]}$$

Moreover, the system can achieve equilibrium for every value of h, and condition [**S29**] therefore implies that

$$g^{\text{eq}}_{ij}(r,h) = g^{\text{eq}}_{ij}(r,1-h). \qquad \textbf{[S30]}$$

To apply Eqs. **S29** and **S30**, let us split the integral over h in Eq. **S28** as

$$\varepsilon_d^{aa} = -\frac{N_a}{2}\int dr \left[\int_0^{1/2} dh \frac{\partial u_{aa}(r,h)}{\partial h} g^{\text{eq}}_{aa}(r,h) + \int_{1/2}^1 dh \frac{\partial u_{aa}(r,h)}{\partial h} g^{\text{eq}}_{aa}(r,h)\right] \qquad \textbf{[S31]}$$

and use $h' = 1 - h$ in the second integral to get

$$\varepsilon_d^{aa} = -\frac{N_a}{2}\int dr \left[\int_0^{1/2} dh \frac{\partial u_{aa}(r,h)}{\partial h} g^{\text{eq}}_{aa}(r,h) - \int_0^{1/2} dh' \frac{\partial u_{aa}(r,1-h')}{\partial h'} g^{\text{eq}}_{aa}(r,1-h')\right]. \qquad \textbf{[S32]}$$

These replacements finally yield

$$\varepsilon_d^{aa} = -\frac{N_a}{2}\int dr \int_0^{1/2} \left(\frac{\partial u_{aa}(r,h)}{\partial h} g^{\text{eq}}_{aa}(r,h) - \frac{\partial u_{aa}(r,1-h)}{\partial h} g^{\text{eq}}_{aa}(r,1-h)\right) dh. \qquad \textbf{[S33]}$$

The combination of Eqs. **S29**, **S30**, and **S33** shows that $\sigma_d \to 0$ for oscillating potentials that are h symmetric and $\tau \to \infty$. Therefore, in our system of particles interacting via time-oscillating potentials, the energy dissipation per period is zero in the high-frequency and slow-frequency limits.

Origin of the Secondary Peak in the σ_d vs. τ Plot for the Dimers Morphology

In Fig. 5 of the main text, we showed that the transition between ordered dissipative structures at high oscillation frequencies and oscillating disordered structures at low frequencies is characterized by a peak in the plot of the energy dissipated per period (σ_d) as a function of the oscillation period (τ). The plot for the dimers (Fig. 5*E*) has a primary peak at $\tau > 100\ t_d$ ascribed to the nonequilibrium order/disorder transition of the dimers and a smaller secondary peak at $\tau \sim 0.2\ t_d$ that, as we show in this section, can be ascribed to the nonequilibrium order/disorder transition of a small population of trimers in the system.

During the formation of dimers from a disordered initial state, some trimers are also formed (one can think of these trimers as kinetically trapped defects in the dimer structure). Fig. S4*A* shows a snapshot of the dimers morphology for a high oscillation frequency where the trimers, which encompass ~8% of the particles in the system, have been highlighted in blue. The trimers give rise to a peak in the *aa* and *bb* pair correlation functions at about 1.9σ (Fig. S3) (the position of the trimer peak is expected at 2σ for linear trimers, but it is observed at smaller distances due to bending). Fig. S4*C* shows the value of the *aa* pair correlation function at the trimer peak as a function of the oscillation period. The trimer peak vanishes with decreasing frequency (Fig. S3), which shows that trimers are stable only for $\tau < 0.1\ t_d$. Interestingly, the inflection point of the plot in Fig. S4*B* is located at the same period ($\sim 0.02\ t_d$) as the secondary peak in the σ_d vs. τ plot (Fig. S4*A*). The order/disorder transition of the trimers is also evidenced by the plot of $\langle\psi_2\rangle_\tau$ (the bond-order parameter of order two) vs. τ, which shows an inflection at $\sim 0.08\ t_d$ (Fig. S4*D*). Note that $\langle\psi_1\rangle_\tau = 1$ and $\langle\psi_2\rangle_\tau = 0$ for a system where all particles form dimers; therefore, the larger $\langle\psi_2\rangle_\tau$ is, the larger the population of trimers (or longer oligomers) in the system. In summary, the trimers in the system present an order/disorder transition at 0.02–0.08 t_d (Fig. S4 *B* and *C*) that we make responsible for the peak at 0.02 t_d in the σ_d vs. τ plot (Fig. S4*A*).

Model of Size-Switching Colloids

We consider a binary system of size-switching particles as an example of dissipative self-assembly via the oscillation of interparticle potentials different from the one presented in the main text. The

system is composed of two types of particles, a and b, which model size-switchable particles, for example pH- or temperature-responsive microgels (4). These particles can be switched between a collapsed state (where the particles are small and sticky) and a swollen-hydrophilic state (where the particles are larger and less sticky than in the collapsed state). We model the interaction energy between these particles, using a 12–6 energy-truncated Lennard-Jones (LJ) potential,

$$u_{\mathrm{LJ}}(r) = \begin{cases} 4\varepsilon\left[\left(\frac{d}{r}\right)^{12} - \left(\frac{d}{r}\right)^{6}\right] - 4\varepsilon\left[\left(\frac{d}{r_{\mathrm{cutoff}}}\right)^{12} - \left(\frac{d}{r_{\mathrm{cutoff}}}\right)^{6}\right] & \text{for } r < r_{\mathrm{cutoff}} \\ 0 & \text{for } r \geq r_{\mathrm{cutoff}}, \end{cases} \quad \textbf{[S34]}$$

where r is the distance between the centers of the particles, ε is the interaction strength (ε is larger for the interaction between two hydrophobic particles than for the interaction between two hydrophilic ones), r_{cutoff} is the cutoff distance (we used 5σ in the calculations), and d is the sum of the radii of the two interacting particles. We denote the time-dependent values of ε and d for the interaction of a particle of type i and one of type j at time t as $d_{ij}(t)$ and $\varepsilon_{ij}(t)$, respectively. We start the simulation ($t = 0$) with particles of type a in the fully collapsed state ($d_{aa} = 0.5\sigma$, $\varepsilon_{aa} = 12.5\ k_{\mathrm{B}}T$) and the particles of type b in the fully swollen state ($d_{bb} = 2.0\sigma$, $\varepsilon_{aa} = 2.5\ k_{\mathrm{B}}T$). For all times (including $t = 0$), we determine the interaction $u_{\mathrm{LJ}}(r)$ between a and b particles, using the combination rules $d_{ab} = (d_{aa} + d_{bb})/2$ and $\varepsilon_{ab} = (\varepsilon_{aa} \cdot \varepsilon_{bb})^{1/2}$. Fig. S5, *Top* shows the interaction potential between the different pairs of particles at $t = 0$.

As time evolves, a swells and b collapses. We model this process by linearly increasing d_{aa} and ε_{bb} and decreasing ε_{aa} and d_{bb} (Fig. S6). For $t = \tau/4$ (where τ is the period of the perturbation), a and b are equivalent (Fig. S5, *Bottom*). For $t = \tau/2$, a is in the completely swollen state and b in the completely collapsed state. At this point, a starts to collapse and b to swell until a full cycle is completed at $t = \tau$. The cycle is then repeated a preestablished number of times.

Fig. S7 *A*–*C* shows the simulated structure of the system upon applying static potentials corresponding to $t = 0$, $\tau/8$, and $\tau/4$, respectively (interparticle potentials in Fig. S5). We observe that for $t = 0$ (Fig. S7*A*), particles of type a form aggregates surrounded by b-type particles. The reason for this behavior is that particles of type a are small and strongly attract each other and will try to phase separate from particles of type b to maximize the number of a–a contacts. We believe that for sufficiently long simulation times, the system in Fig. S7*A* should evolve into a fully phase-separated system. The morphology observed for $t = \tau/8$ (Fig. S7*B*) is similar to that observed for $t = 0$. For $t = \tau/4$ (Fig. S7*C*), particles a and b become identical and therefore form a hexagonal lattice with substitutional disorder.

Fig. S7*D* shows the result of a dynamic simulation for a potential that is oscillated with a period of 0.008 t_{d}. The morphology observed in this case completely differs from those observed in static-potential simulations: The system forms an *ab* square crystal. In other words, the morphology of this dynamic structure cannot be obtained with a static potential corresponding to any given time within the oscillation period. As expected, the dissipative structure obtained for a high-frequency oscillation of the interparticle potentials (Fig. S7*D*) is equivalent to that obtained with a time-averaged effective potential (Fig. S7*E*).

1. Reimann P, Bartussek R, Haussler R, Hanggi P (1996) Brownian motors driven by temperature oscillations. *Phys Lett A* 215(1-2):26–31.
2. Reimann P (2002) Brownian motors: Noisy transport far from equilibrium. *Phys Rep* 361(2–4):57–265.
3. Lahiri S, Jayannavar AM (2009) Total entropy production fluctuation theorems in a nonequilibrium time-periodic steady state. *Eur Phys J B* 69(1):87–92.
4. Lyon LA, Serpe MJ (2012) *Hydrogel Micro and Nanoparticles* (Wiley, Weinheim, Germany).

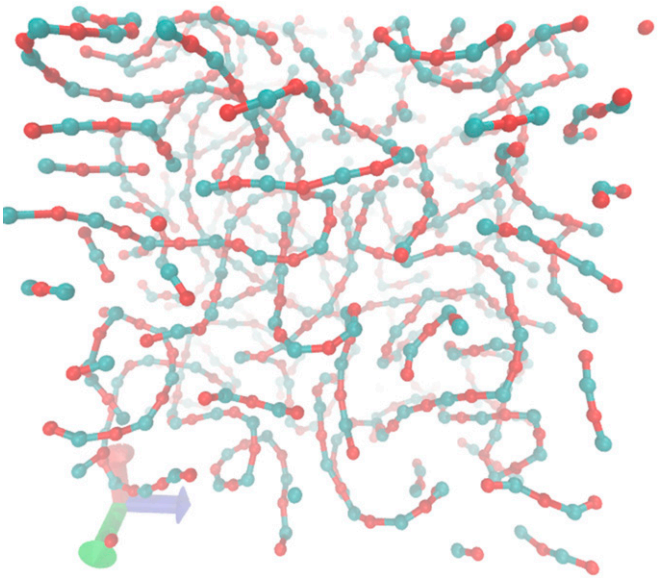

Fig. S1. Simulations in three dimensions produce dissipative structures. Shown is a snapshot of a 3D simulation for the formation of fibers by pH oscillations. Simulation conditions: $C = 1{,}000\ k_BT \cdot \sigma$, $\rho = 0.24$ particles $\cdot\ \sigma^{-3}$, $\tau = 0.08\ t_d$, linear pH–time program (Fig. 3 *B*, *i* of the main text).

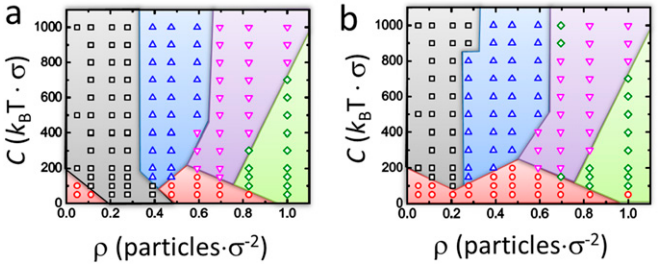

Fig. S2. (*A* and *B*) Morphology diagrams obtained by analysis of the bond-order parameters $\overline{\psi}_n$ (*A*) and by visual inspection of simulation snapshots (*B*).

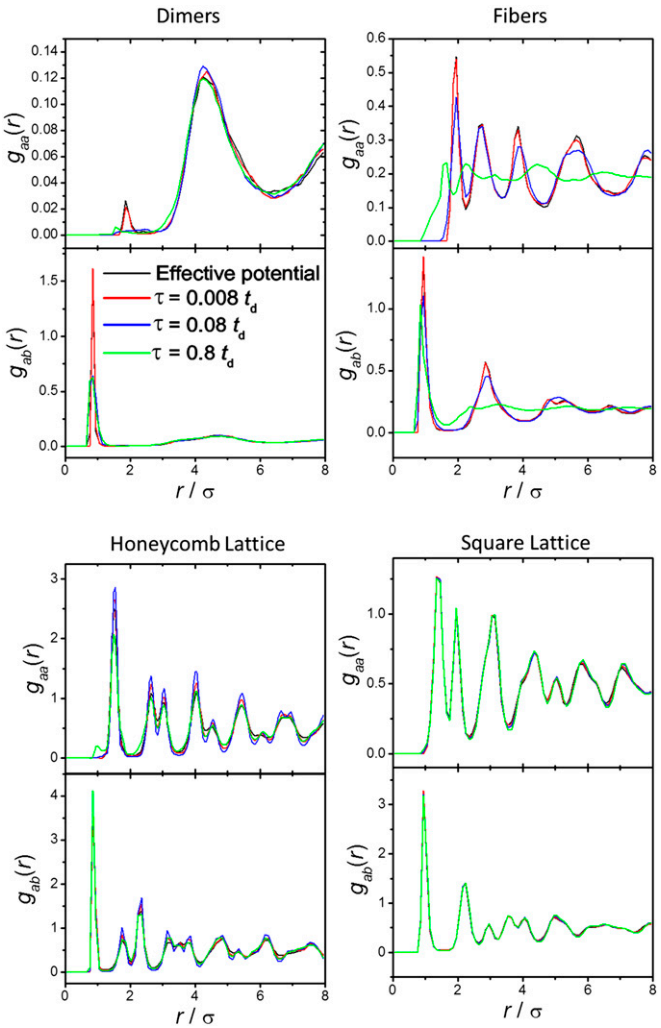

Fig. S3. Pair-correlation functions between *aa* and *ab* pairs of particles for the effective static potential and pH-oscillating potential with different oscillation periods, τ. The pair-correlation function for the pH-oscillating simulations is an average over a full period; therefore $g_{bb}(r) = g_{aa}(r)$. The values of C and ρ for each morphology are the same used for the snapshots in Fig. 3 in the main text.

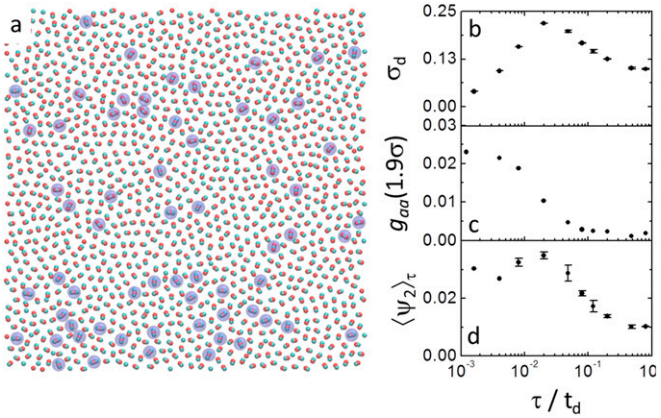

Fig. S4. (*A*) Snapshot of a simulation of the dimer structure ($C = 1{,}000$, $\rho = 0.11$, and $\tau = 0.004\ t_d$). The trimers are highlighted in blue. (*B*) Energy dissipation per oscillation period as a function of the oscillation period (i.e., same plot as in Fig. 5*E* of the main text), showing the secondary peak at $\tau \sim 0.02\ t_d$. (*C*) Intensity of the trimer peak in the pair correlation function of *aa* particles located at $r \sim 1.9\ \sigma$ (Fig. S3) as a function of the oscillation period. (*D*) Period-averaged bond-order parameter of order two, $\langle\psi_2\rangle_\tau$ as a function of the oscillation period. Note that a nonzero parameter $\langle\psi_2\rangle_\tau$ indicates the presence of trimers or longer colloidal molecules.

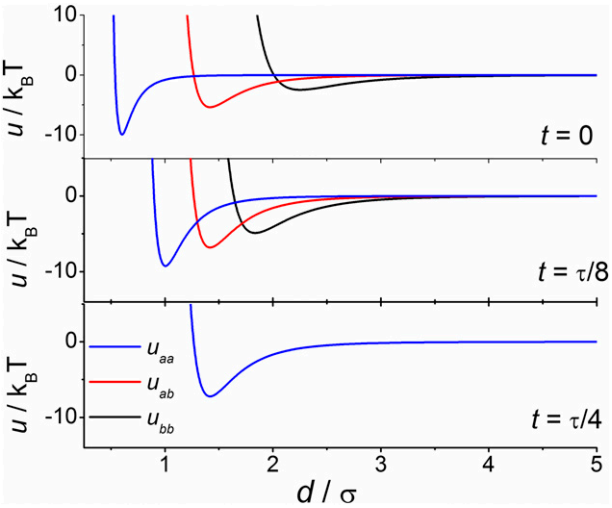

Fig. S5. Interaction potentials between *aa*, *ab*, and *bb* pairs of particles at different times during the oscillation period ($t = 0$, $\tau/8$, and $\tau/4$). For $t = \tau/2$, the potentials are the same as for $t = 0$, but exchanging *a* and *b*. For $t = \tau$, a full cycle is completed and the potentials are the same as for $t = 0$.

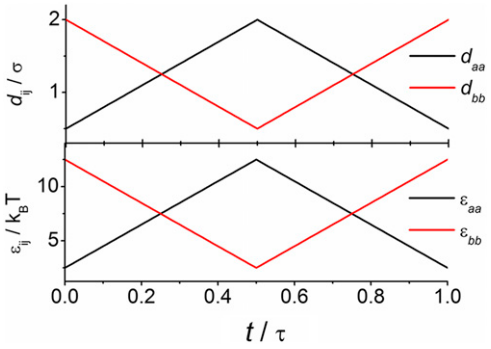

Fig. S6. Values of d_{ij} and ε_{ij} during an oscillating period.

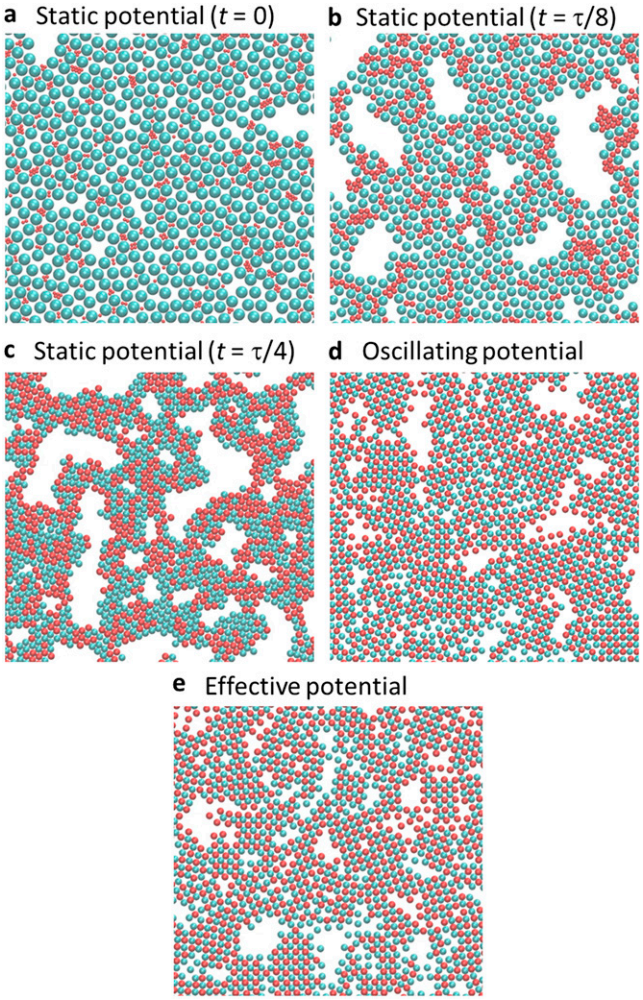

Fig. S7. (*A*–*E*) Snapshots of simulations of size-switchable colloids for different static potentials discussed in the main text (*A*–*C*), the oscillatory potential (*D*) with $\tau = 0.008\ t_d$, and the effective time-averaged potential given by Eq. **5** in the main text (*E*). The density is 0.4 particles $\cdot\ \sigma^{-2}$; *a*-type and *b*-type particles are shown in red and cyan, respectively.

Table S1. Characteristic diffusional timescale for spherical colloids of different size in water at 298 K

σ, colloid size	t_d
1 nm	3 ns
10 nm	3 μs
100 nm	3 ms
1 μm	3 s
10 μm	3,000 s